1 **Fine-scale oceanographic drivers of reef manta ray (*Mobula alfredi*) visitation patterns at a**

2 **feeding aggregation site**

3 **Running head:**

4 Drivers of reef manta ray visitation patterns

5 **Author List:**

6 Joanna L. Harris [a, b*], Phil Hosegood [b], Edward Robinson [b], Clare B. Embling [b], Simon

7 Hilbourne [a], Guy M. W. Stevens [a]

8

9 **Author Affiliations:**

10 [a] The Manta Trust, Catemwood House, Norwood Lane, Corscombe, Dorset, DT2 0NT, UK

11 [b] School of Biological and Marine Sciences, University of Plymouth, Drake Circus, Plymouth

12 PL4 8AA, UK

13 ***Corresponding Author**:

14 joanna.l.harris@plymouth.ac.uk (Corresponding author – Joanna L. Harris)

15 +44 7480 717 199

16

17 **Co Author Contacts:**

18 phil.hosegood@plymouth.ac.uk (Phil Hosegood), edward.robinson@plymouth.ac.uk

19 (Edward Robinson), clare.embling@plymouth.ac.uk (Clare Embling), simon@mantatrust.org

20 (Simon Hilbourne), guy@mantatrust.org (Guy Stevens)

21 **Abstract**

22 Globally, reef manta rays (*Mobula alfredi*) are in decline and are particularly vulnerable to

23 exploitation and disturbance at aggregation sites. Here, passive acoustic telemetry and a suite

24 of advanced oceanographic technologies were used for the first time to investigate the fine-

25 scale (5-min) influence of oceanographic drivers on the visitation patterns of 19 tagged *M.*

26 *alfredi* to a feeding aggregation site at Egmont Atoll in the Chagos Archipelago. Boosted

27 regression trees indicate that tag detection probability increased with the intrusion of cold-

28 water bores propagating up the atoll slope through the narrow lagoon inlet during flood tide,

29 potentially transporting zooplankton from the thermocline. Tag detection probability also

30 increased with warmer near-surface temperature close to low tide, with near-surface

31 currents flowing offshore, and with high levels of backscatter (a proxy of zooplankton

32 biomass). These combinations of processes support the proposition that zooplankton carried

33 from the thermocline into the lagoon during the flood may be pumped back out through the

34 narrow inlet during an ebb tide. These conditions provide temporally limited feeding

35 opportunities for *M. alfredi,* which are tied on the tides. Results also provide some evidence

36 of the presence of Langmuir Circulation, which transports and concentrates zooplankton, and

37 may partly explain why *M. alfredi* occasionally remained at the feeding location for longer

38 than that two hours. Identification of these correlations provides unique insight into the

39 dynamic synthesis of fine-scale oceanographic processes which are likely to influence the

40 foraging ecology of *M. alfredi* at Egmont Atoll, and elsewhere throughout their range.

41

Introduction

Reef manta rays (*Mobula alfredi*) are large zooplanktivorous elasmobranchs of the family Mobulidae (Hosegood *et al.,* 2020; Marshall *et al.*, 2009; White *et al.*, 2017). The global population is widely distributed in highly fragmented subpopulations throughout tropical and sub-tropical waters of the Indo-West Pacific Oceans (Couturier *et al.*, 2012; Marshall *et al.*, 2019). Subpopulations appear to have limited home ranges, typically centred around coral reef ecosystems (McCauley *et al.*, 2014; Kessel *et al.*, 2017; Couturier *et al.*, 2018; Setyawan *et al.*, 2018). Aggregation behaviour is characteristic of the species, whereby subpopulations will concentrate the majority of their activities at certain 'hotspot' locations (Couturier *et al.*, 2018; Setyawan *et al.*, 2018; Harris *et al.*, 2020). These aggregations typically occur within particular discrete habitats (Stevens, 2016; Harris *et al.*, 2020) such as cleaning stations (O'Shea *et al.*, 2010), and locations where they engaged in social (Stevens, 2016; Perryman *et al.*, 2019) or reproductive activities (Stevens *et al.*, 2018). Large feeding aggregations also occur, and are often associated with the species' reliance on dense assemblages of prey (Armstrong *et al.*, 2016) in a largely oligotrophic environment (Morel *et al.*, 2010).

Extensive targeted and bycatch fisheries of *M. alfredi,* driven in part for their gill plates [pre-branchial appendages, used to filter their zooplankton prey from the water (Paig-Tran *et al.*, 2013), which are utilised in the Asian medicinal trade (O'Malley *et al.*, 2017)], has led to dramatic subpopulation declines in recent decades (Couturier *et al.*, 2013; Lawson *et al.*, 2017; Rohner *et al.*, 2017; Marshall *et al.*, 2019). Population recovery from such exploitation is hindered by their conservative life-history traits; the species are slow-growing,

66 late to mature and only have a few offspring in their lifetime (Dulvy *et al.*, 2014; Stevens,

67 2016).

68   *Mobula alfredi* are particularly vulnerable to exploitation and changes in climate at

69 feeding aggregation sites. For example, anthropogenic disturbance may reduce individual *M.*

70 *alfredi* fitness by driving them away from productive feeding areas (Venables *et al.*, 2016;

71 Murray *et al.*, 2019), which has been highlighted as a major conservation concern for the

72 species (Murray *et al.*, 2019; Harris *et al.*, 2020). Feeding behaviour may also be disrupted by

73 enhanced stratification driven by rising sea surface temperatures, which can decrease marine

74 phytoplankton (Roxy *et al.*, 2016), and with it zooplankton biomass (Richardson, 2008).

75   Studies which investigate *M. alfredi* aggregation behaviour have associated their

76 occurrence with various broadscale physical factors, such as wind speed, moon phase, sea

77 surface temperature, and tidal phase (Dewar *et al.*, 2008; Jaine *et al.*, 2012; Couturier *et al.*,

78 2018; Peel *et al.*, 2019b). However, the fine-scale changes in the oceanographic environment

79 that potentially drive feeding aggregations have yet to be investigated.

80   Situated in the central Indian Ocean, the Chagos Archipelago (Figure 1) has been

81 uninhabited for many decades (excluding Diego Garcia Atoll) (Sheppard *et al.*, 2012). Due to

82 the lack of human influence, such as coastal development and anthropogenic pollution, the

83 region is considered virtually pristine (Readman *et al.*, 2013). Owing to the region's unique

84 marine environment, a no-take marine protected area (MPA), which encompasses the entire

85 exclusive economic zone (EEZ) (640,000km^2) except for a 3nm exclusion around the boundary

86 of Diego Garcia Atoll, was established in 2010 (Sheppard *et al.*, 2012). The archipelago

87 supports a subpopulation of *M. alfredi* which is largely undocumented due to the remoteness

88 of the location and strict protective measures; as is the region's physical oceanographic

89   environment (Hosegood *et al.*, 2019). Broadscale studies conducted in the region indicated

90   that Egmont Atoll, situated in the southwest of the archipelago, provides key habitats for this

91   *M. alfredi* subpopulation (Harris, 2019; Andrzejaczek *et al.*, 2020). Feeding *M. alfredi* are

92   regularly observed around the atoll (Harris, 2019); behaviour which is thought to be

93   associated with shallow bathymetry, low current speeds, and cooler sea surface temperatures

94   (Jaine *et al.*, 2012; Armstrong *et al.*, 2016; Couturier *et al.*, 2018; Harris, 2019; Peel *et al.*,

95   2019b). Together, these factors may act to induce upwelling of nutrients, increasing primary

96   and secondary production (McManus *et al.*, 2005). Furthermore, currents interacting with

97   topography may aggregate zooplankton (Genin *et al.*, 2005), resulting in highly productive

98   feeding grounds for a range of species, including *M. alfredi* (Hosegood *et al.*, 2019).

99   Field observations have identified an *M. alfredi* feeding aggregation 'hotspot' at the

100   north of Egmont Atoll (Harris and Stevens, unpublished data). However, *M. alfredi* feeding

101   activity can be dramatically different from one day to another, with little apparent change in

102   broadscale oceanographic conditions (Harris, 2019). Therefore, a greater understanding of

103   how *M. alfredi* respond to fine-scale environmental drivers is needed. Here, passive acoustic

104   telemetry and *in situ* oceanographic monitoring is used to investigate *M. alfredi* activity at

105   Egmont Atoll, and assess what physical factors drive fine-scale (5-min) visitation patterns at

106   the observed feeding aggregation hotspot. This study aims to enhance the current

107   understanding of *M. alfredi* foraging ecology by providing detailed insight into their fine-scale

108   movement patterns in response to natural changes in their oceanographic environment.

109   **Methods**

110   *Study site*

111   The Chagos Archipelago is comprised of seven atolls, several large submerged banks and

112   more than 60 low lying islands, located at the southernmost end of the Lakshadweep–

113   Maldives–Chagos ridge; 450km south of the Maldives (Sheppard *et al.*, 2012) (Figure 1).

114   Egmont Atoll's geomorphology is typical of an atoll with an interior lagoon system which is

115   separated from the open ocean by reef crests and flats, with narrow connecting channel

116   systems (Woodroffe and Biribo, 2011). During six expeditions, between January 2015 and

117   December 2019 (Harris and Stevens, unpublished data), the authors repeatedly observed

118   aggregations of *M. alfredi* engaged in feeding activity at a site called Manta Alley (Figure 1).

119   At this foraging hotspot, using in-water observations (Figure 2) and ROVs, *M. alfredi* were

120   recorded feeding at the surface and down to a depth of 120 m (Harris and Stevens,

121   unpublished data; Diaz and Foster, unpublished data). Manta Alley is located 100 m north of

122   Egmont Atoll's northeast rim, where two narrow (<350 m) passages are situated. From the

123   shallow lagoon passages (<5 m), the topography slopes steeply down (up to 47°) before

124   reaching a 50 m wide plateau 80 m from the lagoon, with a depth of 65-71 m. On the seaward

125   side, there is a narrow ridge which inclines steeply (up to 39°) to a height of approximately 10

126   m, followed by another sharp slope down to >100m (Robinson and Hosegood *et al.*,

127   unpublished data) (Figure 1).

128   *Oceanographic Moorings*

129   Two instrumented oceanographic moorings were deployed in Manta Alley (Figure 1)

130   from a research ship on 30th December 2019. Both moorings were positioned within Manta

131   Alley. The first was a subsurface taut-line mooring deployed in 66 m, with the uppermost

132   buoyancy element at a depth of 20 m. Temperature was measured by RBRSolo^{3}T temperature

133   sensors positioned at 2 m intervals from 4 m to 48 m above the seabed. In addition to the

134   temperature sensors, RBR Concerto conductivity-temperature-depth (CTD) sensors with a

135   sampling interval of 5s were positioned at 2 m and 50 m above the bed. An acoustic receiver

136   (see *acoustic receiver array* section below) was positioned approximately 7 m below the near-

137   surface CTD, at 43 m above the bed. The second mooring, deployed 182 m southeast of the

138   first, comprised an upward-facing Nortek Signature 500kHz acoustic Doppler current profiler

139   (ADCP), mounted on a subsurface buoy 3 m above the seabed. Both moorings were recovered

140   on 17th March 2020; however, the Nortek Signature 500kHz ADCP had ceased sampling on

141   10th March 2020.

142   *Acoustic tag deployment*

143   Tagging activities were carried out at Egmont Atoll between 19th November 2019 -

144   3rd December 2019 while freediving. Twenty VEMCO V16-4x acoustic transmitter tags

145   (Vemco Inc., Nova Scotia, Canada), each tethered to a titanium anchor (Wildlife Computers)

146   with a small diameter cable, were deployed on the right dorsal musculature using a modified

147   Hawaiian hand sling while swimming behind the *M. alfredi*. Each tag was set to operate at 69

148   kHz and transmit a unique acoustic signal at random intervals between 30 and 90 seconds.

149   Before being tagged, the ventral side of each *M. alfredi* was photographed to capture their

150   unique spot pattern for identification purposes (Marshall and Pierce, 2012), and their sex and

151   size class (a proxy of maturity status) were recorded (Stevens, 2016). Five of the twenty *M.*

152   *alfredi* that were tagged were re-sighted at their tagging locations between three and 12 days

153   after deployment. All five were observed to be engaged in normal feeding activities (Stevens,

154   2016). All activities were approved by the University of Plymouth Animals in Science Ethics

155   Committee under permit ETHICS-24-2019.

156   *Acoustic receiver array*

157   An acoustic array of five VR2W-69 kHz omnidirectional acoustic receivers (Vemco Inc.,

158   Nova Scotia, Canada) were deployed at depths ranging from 12 to 22 m below the sea surface

159   on the reef flat close to the reef slope at sites corresponding to known *M. alfredi* aggregation

160   areas around the outer rim of Egmont Atoll (Figure 1). Four of the receivers were suspended

161   approximately 2 m above the seabed, while the fifth was attached to an oceanographic

162   mooring 43 m above the seabed at the Manta Alley aggregation site. Acoustic tags were

163   detected within approximately 160 m of the receivers: mean = 162 ± 31 m (SD) as determined

164   by range testing conducted following the method described by Lea (2017).

165   *Acoustic tag analysis*

166   All tag detection data was imported into VUE software (version 2.6.2) and filtered for

167   active tags. The False Detection Analyser (VUE version 2.6.2) was then used to identify false

168   detections, whereby the ratio of short and long periods between detections is calculated from

169   the time between detections on each receiver (Simpfendorfer *et al.*, 2015)**.** Here, the default

170   short to long periods of <30 min and >12 h, respectively were used (Simpfendorfer *et al.*,

171   2015) and all detections suspected to be false were removed from analysis**.** The percentage

172   of sightings at each location were then projected in ArcGIS 10.7.

173   To assess whether Egmont Atoll can be considered a key habitat, residency indices (RI)

174   were calculated using the following form (Peel *et al.*, 2019b), allowing comparison of

175   residency patterns at Egmont Atoll between *M. alfredi* regardless of differences in tracking

176   periods (Daly *et al.*, 2014)**.**

177
$$RI(\%) = \frac{Number\ of\ days\ detected}{Number\ of\ days\ between\ first\ and\ last\ detection}\ x\ 100$$

178   To assess the intensity at which locations were utilised, the amount of time each

179   tagged *M. alfredi* spent within the detection range of each acoustic receivers was calculated

180   using the VTrack R package (Campbell *et al.*, 2012) in R 3.5.2 (R Core Team, 2018). Briefly,

181   each tag detection was classed as a resident or non-resident events. A resident event began

182   when there were two or more successive detections (Nalesso *et al.*, 2019) at the same

183   receiver within 60 minutes. Termination of the resident event occurred at the time of the last

184   detection when there were no further detections within 60 minutes, or when the tag was

185   detected at least twice at another receiver (Campbell *et al.*, 2012; Nalesso *et al.*, 2019).

186   *Environmental Influences: Boosted regression trees*

187   Boosted regression trees (BRT) were used to investigate the relationship between

188   environmental variables and the visitation patterns of tagged *M. alfredi* to the feeding

189   aggregation site at Manta Alley. The modelling technique is based on two algorithms:

190   regression trees models and boosting, which build and combine large numbers of relatively

191   small trees by fitting each new tree to the residuals of the last (Elith *et al.*, 2008). Each tree is

192   constructed through a series of binary splits of predictor variables (Hastie *et al.*, 2009), which

193   occur based on the homogeneity of their relationship to the response variable (Colin *et al.*,

194   2017). Multiple splits are tested, and partitioning occurs when the greatest improvement of

195   homogeneity is found (Colin *et al.*, 2017). Advantages of this modelling technique include its

196   ability to fit complex, non-linear relationships, model interactions between response

197   variables (Elith *et al.*, 2008), and the appropriate data model does not require assumptions

198   about the residuals of the model (Derville *et al.*, 2016).

199   Detection data was divided into a time-series of 5-min bins starting from 1st December

200   2019 and ending on 10th March 2020. The BRT was then constructed with a binomial response

201   of present (1) or absent (0) within each 5-min bin. The final time-series contained 28654 x 5-

202   min bins of presence and absence observations.

203   Nine predictor variables representing temperature (1-2), zooplankton biomass (3),

204   ocean currents (4-8), and tide (9), all of which have been shown to influence *M. alfredi*

205   occurrence (O'Shea *et al.*, 2010; Anderson *et al.*, 2011; Harris *et al.*, 2020) were selected for

206   inclusion (Table 1). Temperature variables included: temperature at 2 m above the seabed

207   (temp 2 m) (1), and 50 m above the seabed (temp 50 m) (2), sampled every 5s using RBR

208   Concerto CTDs. Data were pooled into the same 5-min bins as the presence and absence data.

209   The mean temperature for each 5-min bin was then calculated from the 60 data points. For

210   zooplankton biomass (3), acoustic backscatter was used as a proxy. Data were taken from

211   beam 1 of the Nortek Signature 500kHz ADCP, aligned with x positive and a centre frequency

212   of 500kHz with a bandwidth of 25kHz and retrieved from the Nortek Average AD2CP file with

213   a sample interval of 10 mins. The instrument has a vertical resolution of 2 m per bin, and the

214   first 25 bins were taken for data processing (0.5-50.5 m range from the instrument). The

215   vertical profile at each time step was filtered with a running median window with a length of

216   3 and a maximum deviation of 1. These parameters were chosen based on observations in

217   the data that any areas of amplified return (likely due to large targets which are not

218   zooplankton) were constrained to the extent of a single bin due to the relatively large size of

219   the 2 m bins when compared to the observed target size. A depth-mean value was then

220   calculated for each time step and linearly interpolated into the 5-min bins. Ocean current data

221   (4) included vertical velocity, for which a depth mean was calculated from the same average

222   data and bin selection as backscatter, but with no filtering applied due to the low noise level

223   in averaged velocity measurements. Data were then interpolated on to a 5-min time scale.

224   Ocean current data also included the eastward (u) component at 8.5 m and 48.5 m above the

225   seabed, and northward (v) component 8.5 m and 48.5 m above the bed. Data were obtained

226   from the Nortek Average AD2CP file, which provides a reading of component velocity at 10-

227   min intervals; each reading covers a time period of 120 seconds and is composed of 48

228   independent samples (0.4 Hz), giving an overall measurement uncertainty of <1 cm s^{-1} for

229   horizontal velocity measurements. Ten-min data were interpolated onto a 5-min timescale

230   using linear sampling. Each variable is representative of a single 2 m depth bin, chosen to be

231   safely out of the influence range for ringing and sidelobe interference (5.5m and 45.5 m from

232   the transducer, respectively). Both u and v velocity components were then rotated clockwise

233   117° relative to north, to align with the slope in Manta Alley (adjusted positive and negative

234   directions, shown in Figure 3), resulting in the ocean current predictor variables: cross-shore

235   current at 48.5 m above the bed (CS current (v) 48.5 m) (5), cross-shore current at 8.5 m above

236   the bed (CS current (v) 8.5 m) (6), longshore current at 48.5 m above the bed (LS current (u)

237   48.5 m) (7), and longshore current at 8.5 m above the bed (LS current (u) 8.5 m) (8). To

238   estimate tidal phase, pressure data was taken from the lower RBR Concerto CTD (depth 64.1

239   m) and converted to depth data using RSKTools inbuild conversion function. Data were

240   cleaned with a median filter and averaged with a running window (both size 501 points). The

241   Matlab inbuilt find peaks function was then used and ran twice to pick out both high and low

242   tides by inverting the data on one run. A 5.5 h minimum peak spacing was specified to further

243   reduce susceptibility to noise, and the resulting data points were visually validated against

244   the raw depth data. The variable time relative to high tide (9), was then calculated with high

245   tide as zero and negative hours before (flood) and positive hours after (ebb) (Peel *et al.*,

246   2019b).

247   All models were fitted using the gbm.step() function of the dismo R package (Hijmans

248   *et al.*, 2017). Initial models were built to find suitable settings for four parameters: tree

249   complexity (*tc*), which specifies the number of interactions that should be modelled, learning

250   rate (*lr*), which regulates the contribution of each tree to the growing model, bag fraction (*bf*),

251   which controls stochasticity by randomly selecting (without replacement) a specified subset

252   of the data at each iteration and step size (*ss*), which controls the number of trees which

253   should be added at each iteration (Elith *et al.*, 2008). The following parameter settings were

254   tested: *tc* = 1-6, *lr* = 0.01, 0.005, 0.001 and 0.0001, *bf* = 0.5, 0.7, 0.9, *ss* = 25 and 50, resulting

255   in 144 models.

256   Ten-fold cross-validation (CV) was applied to assess model performance, whereby the

257   model is fitted to training data and then is tested against a withheld portion (hold-out sample)

258   of the dataset (Elith *et al.*, 2008). The model's ability to fit the withheld data was then

259   measured by comparing the area under the receiver operating characteristic curve (AUC) test

260   statistic (Froeschke *et al.*, 2010; Dedman *et al.*, 2017) for both the training data ($_T$AUC) and

261   hold-out sample (cross-validation AUC, $_{CV}$AUC) (Dedman *et al.*, 2017; Elith and Leathwick,

262   2017). The AUC classification ranges from 0 - 1, whereby: < 0.5 (fail), 0.6 – 0.7 (poor), 0.7 –

263   0.8 (acceptable), 0.8 – 0.9 (excellent), > 0.9 (outstanding) (Hosmer and Lemeshow, 2000). The

264   difference between the $_T$AUC and the $_{CV}$AUC (ΔAUC) indicates the level of overfitting of the

265   primary sample (Dedman *et al.*, 2017). Therefore, better model performance is categorised

266   by higher AUC values for both $_T$AUC and $_{CV}$AUC, but a lower ΔAUC (Dedman *et al.*, 2017).

267   The percentage of deviance explained by the model was determined using the pseudo

268   determination coefficient (D^2), calculated using the following form (Nieto and Mélin, 2017):

269     $$D^2 = 1 - (residual\ deviance/\ total\ deviance)$$

270   The final model was fitted with *tc* = 6, *lr* = 0.005, *bf* = 0.7, and *ss* = 50 (Table S2). The

271   relative contribution of predictor variables to the BRT model is measured by averaging the

272   number of times a variable is chosen for splitting and the squared improvement resulting

273   from these splits (scaled to 100 across all the variables) (Elith *et al.*, 2008). To ensure non-

274   informative predictors were not hindering model performance, pairwise correlation

275   coefficients and variance inflation factor (VIF) estimates (Jouffray *et al.*, 2019) were

276   calculated, all were in an acceptable range; coefficients < 0.6 and/or VIF estimates < 3.5

277   (Jouffray *et al.*, 2019) (Table S1 and Figure S1).

278   Due to the complex nature of BRTs, model results cannot be easily visualised.

279   Therefore, partial dependency and interaction plots were generated for interpretation. The

280   plots display the results of the predicted effect on tag detection probability for a given

281   predictor, or pair of predictors, after accounting for the mean effects of all other predictors

282   (Elith *et al.*, 2008; Hastie *et al.*, 2009). Confidence intervals (95%) for the partial dependency

283   plots were obtained from 1000 bootstrap replicates (Jouffray *et al.*, 2019). For interaction

284   plots, 100 bootstrap resampling was used to test the significance of the strongest interactions

285   (Pinsky and Byler, 2015; Jouffray *et al.*, 2019) (interaction strength > 100) by randomly

286   sampling the occurrence of *M. alfredi* at each location before re-fitting the BRT models

287   (Jouffray *et al.*, 2019). The size of the interaction was then used to generate a distribution

288   under the null hypothesis of no interaction among predictors (Jouffray *et al.*, 2019).

289   **Results**

290   *Detection and resident event summary*

291   Acoustic transmitter tags were deployed on eleven female (adults = 5, sub-adults = 4,

292   juvenile = 2) and nine male (adults = 3, juvenile = 6) *M. alfredi* (Table 2). Nineteen of the 20

293   tags returned useable tracks (Table 2). No detections have been recorded for three of the 19

294   tags since 21st November 2019 (CG-MA-0120), 27th December 2019 (CG-MA-0161), and 20th

295   January 2020 (CG-MA-0141). However, it is not possible to distinguish between acoustic tag

296   loss and emigration from the study area, and relatively long temporal gaps between

297   detections of *M. alfredi* in the Chagos Archipelago have previously been reported

298   (Andrzejaczek *et al.*, 2020). Therefore, the current status of these tags has been recorded as

299   'unknown' rather than 'inactive', pending further data collection.

300   There were a total of 15965 detections during the study period (Table 2). The highest

301   percentage of detections occurred at the acoustic receiver deployed on the oceanographic

302   mooring in Manta Alley (51.4%), followed by North IdR Cleaning Station (22.3%) (Figure 4).

303   The overall distribution of detections by hour of the day shows 70.9% of detections

304   occurred at Egmont Atoll during the day (06:00-18:00) (Figure 5). For adults, only 18.3% of

305   detections occurred at night (19:00-05:00), while 35% of detections occurred at night for

306   juveniles.

307   The mean total time between tag deployment when the tags first began transmitting

308   until the end of the study, when the detection data was downloaded was 113 ± 5 day (range

309   106-119 days). During this time, tagged *M. alfredi* were tracked (first to last tag detection) for

310   a mean of 97 ± 32 days (range 3 – 116 days), with a mean of 50 ± 23 detection days (range 2-

311   92 days). Residency indices show that tagged *M. alfredi* were detected at Egmont Atoll for a

312   mean of 52% of the days they were tracked (RI = 52 ± 15.7%), with a minimum and maximum

313   RI of 24% and 80.3%, respectively (Table 2). Mean residency indices were similar for both

314   adults and juveniles (including sub-adults), which were 53 ± 16% and 51 ± 16%, respectively.

315   Overall, 2074 resident events were recorded for 19 *M. alfredi* (Figure 6). The highest

316   number of resident events occurred at Manta Alley (837), totalling 22188 mins (369.8 hrs).

317   Manta Alley also had the longest individual mean resident event time (27±51, Table 3), with

318   the longest resident event of 489 min (8.2 hrs) by a juvenile male (manta-ID CG-MA-0125). Of

319   the 837 resident events, a total of 35 lasted >120 mins, of which 11 were female (adult = 5,

320   juvenile = 6) and 24 were males (adult = 3, juvenile =21).

321   The lowest number of residency events occurred at Ile Sudest (41), totalling 191 mins

322   (3.1 hrs). Mean resident event time was 5 ± 10 mins, with a maximum resident event time of

323   56 mins by an adult male (manta-ID CG-MA-0161).

324   *Environmental Influences: Boosted regression trees*

325   Model performance evaluation for the BRT, including all nine predictors, had

326   outstanding and excellent predictive performance for the training ($_T$AUC = 1) and cross-

327   validated ($_{CV}$AUC = 0.89) data, respectively, with minimal evidence of overfitting (ΔAUC =

328   0.11). The estimated D^2 suggests that 72 % of the deviance was explained (Table S2).

329   Partial dependency plots (Figure 7) indicate that the probability of detections

330   decreased with increased near-bed temperature (temp 2 m, 16.2%), and increased with

331   increased backscatter strength (13.3%) and near-surface temperature (temp 50 m, 13.3%).

332   Detection probability was higher with greater downward vertical velocity (12.8%), and during

333   the early stages of a flood tide (12.1%), approximately two hours following low tide when

334   near-surface longshore current velocity (longshore (v) 48.5 m, 11.7%) was approximately 0.2

335   ms^{-1} near the surface and 0.3 ms^{-1} near the seabed (longshore (v) 8.5 m, 9.1%). For cross-

336   shore currents, detection probability increased when near-surface currents were flowing

337   offshore (cross-shore (u) 48.5 m, 6.1%) at approximately -0.05 m s^{-1}, and when near-bed

338   currents (cross-shore (u) 8.5 m, 5.4%) were flowing inshore at approximately 0.15 ms^{-1}.

339   Eight significant pairwise interactions occurred between eight predictors (Table 4 and

340   Figure S2). These interactions should not be considered in isolation, as they may arise

341   separately or simultaneously, and may be affected by other variables. However, they provide

342   insight into the estimated influence of several paired-environmental processes which can

343   increase the probability of tag detections. For example, tag detections probability was highest

344   when upward currents speed (vertical velocity) was increased, and the near-surface

345   temperature (Figure S2a) was warmer (temp 50 >29.5°C). Tag detection probability also

346   increased with cooler near-bed temperature (temp 2 m <24°C), and increased near-surface

347   temperatures (temp 50 m >29.5°C) (Figure S2b). It also increased when near-bed cross-shore

348   currents (cross-shore (u) 8.5 m) were of a high +ve velocity (>0.15ms^{-1}) (flowing into the

349   lagoon) and backscatter was > 55 (Figure S2c), and with high temp 2 m (> 29°C) and

350   backscatter > 55 (Figure S2d).

351   **Discussion**

352   Overall, *M. alfredi* residency at Egmont Atoll, measured by the residency index (RI),

353   was high (mean RI =52%), which supports previous reports that Egmont Atoll provides key

354   habitats for this species (Harris, 2019; Andrzejaczek *et al.*, 2020). Similar high levels of

355   residency have been observed in the Red Sea (mean RI = 65%) (Braun *et al.*, 2015) and at the

356   Amirante Islands of Seychelles (mean RI = 62%) (Peel *et al.*, 2019b). Adult and juvenile *M.*

357   *alfredi* displayed similar residency at Egmont Atoll, which is in contrast to patterns observed

358   in Seychelles, where the RI was lower for adults (Peel *et al.*, 2019b), indicating that the *M.*

359   *alfredi* habitat at Egmont Atoll is perhaps consistently important for all life stages.

360   Alternatively, the similar residency of adults and juveniles could be attributed to the acoustic

361   array design (Peel *et al.*, 2019b). To establish a more robust RI, future research would benefit

362   from increased spatial coverage, including the deployment of acoustic receivers in locations

363   which may be frequented by juveniles such as inside the lagoon.

364   Overall, detection data displays diel behaviour patterns, with the highest percentage

365   of detections at Egmont Atoll occurring during the day. Similar diel patterns have been

366   recorded during studies of various *M. alfredi* subpopulations, where individuals frequented

367   shallow coastal and island reef systems more often during daylight hours (Dewar *et al.*, 2008;

368   Jaine *et al.*, 2012; Couturier *et al.*, 2018; Setyawan *et al.*, 2018; Peel *et al.*, 2019b). These

369   patterns may be associated with the species use of cleaning stations, where cleaner fish are

370   only active during the day (Côté, 2000). Diel movement patterns may also be associated with

371   efficient foraging strategies. For example, *M. alfredi* may predominately frequent shallow reef

372   habitats during the day to feed on reef-associated zooplankton which can accumulate in

373   surface waters over shallow reefs when avoiding predation from reef-dwelling diurnal

374   consumers (Alldredge and King, 2009; Leichter *et al.*, 2013). At night, *M. alfredi* may then

375   travel offshore to forage (Dewar *et al.*, 2008; Jaine *et al.*, 2012; Couturier *et al.*, 2018) when

376   diel vertically migrating zooplankton ascends into warmer water (Dewar *et al.*, 2008; Braun

377   *et al.*, 2014; Couturier *et al.*, 2018). This hypothesis is supported by stable isotope analysis,

378   which indicates that a large proportion of *M. alfredi* diet is made up of both near-surface and

379   demersal zooplankton (Couturier *et al.*, 2013b; Peel *et al.*, 2019a). The diel *M. alfredi*

380   movement pattern was less pronounced for juveniles, which were more frequently detected

381   at night than adults, suggesting that juvenile *M. alfredi* remain in shallower reef habitats

382   longer. This pattern has also been observed in other subpopulations and is likely a predator

383   avoidance strategy by the more vulnerable juveniles (Cerutti-Pereyra *et al.*, 2014; Stewart *et

384   al.*, 2018; Peel *et al.*, 2019b). Their smaller body size may also make it less energetically

385   efficient for juveniles to travel offshore (Nøttestad *et al.*, 1999; Peel *et al.*, 2019b), and/or

386   their foraging experience may be limited (Peel *et al.*, 2019b).

387   Manta Alley had the highest number of detections, and there were repeated resident

388   events for 18 of the 19 tagged individuals, indicating a high level of site fidelity. Site fidelity is

389   a well-reported characteristic of *M. alfredi,* having been observed in photographic

390   identification, acoustic telemetry and satellite tagging studies (Dewar *et al.*, 2008; Deakos,

391   2011; Jaine *et al.*, 2014; McCauley *et al.*, 2014; Stevens, 2016; Kessel *et al.*, 2017; Couturier *et*

392   *al.*, 2018). Site fidelity has been attributed in part to the species' reliance on specific

393   habitats, which provide a sufficient food resource, protection from predation, and

394   opportunities to clean, socialise and reproduce (Jaine *et al.*, 2014; McCauley *et al.*, 2014;

395   Stevens, 2016; Perryman *et al.*, 2019). Resident events were longer at Manta Alley than at

396   any other location. The depth of the majority of the area within the range of the acoustic

397   receiver is greater than 40 m. As 40 m is the maximum depth of occurrence for cleaner fish in

398   the Chagos Archipelago (Kuiter, 2014), it is unlikely that these extended resident events at

399   Manta Alley are associated with cleaning activities. Furthermore, in-water observations at this

400   site by the authors during this study observed large *M. alfredi* aggregations feeding (~40

401   individuals) on the surface down to 20 m on several occasions, while no cleaning stations were

402   identified. Therefore, the most likely driver of the visitation patterns recorded for *M. alfredi*

403   at this site during this study is foraging opportunities. For *M. alfredi* foraging activities to be

404   energetically efficient, high densities of prey are required (Armstrong *et al.*, 2016). The BRT

405   model suggests that *M. alfredi* presence at Manta Alley is associated with various fine-scale

406   oceanographic processes, which could be combining to enhance localised zooplankton

407   abundance.

408   A high tag detection probability of *M. alfredi* occurred with cold near-bed and warm

409   near-surface temperature, and probability increased with increasing difference between

410   these temperatures. Extreme short-term fluctuations in near-bed temperatures may be

411   associated with the intrusion of cold-water created by internal waves which disrupt the

412   thermocline (Shanks *et al.*, 2014). Enhanced concentrations of zooplankton often occur at the

413   thermocline, the thickness of which can be increased by internal waves (McManus *et al.*,

414   2005*).* These internal waves break as they interact with the steep slope of an atoll leading to

415   the formation of cold-water bores which propagate up the slope (Woodson, 2018; Hosegood

416   *et al.*, 2019). Bores enhance the upward transport of organisms, and thus the concentration

417   in surface waters (Stevick *et al.*, 2008), which may provide efficient foraging opportunities for

418   the zooplanktivorous *M. alfredi.* The upward propagation of cold-water bores has been

419   observed to vary tidally (Leichter *et al.*, 1996; Hosegood *et al.*, 2019), and can become more

420   frequent during a flood tide leading to a pulsed delivery of organisms (Leichter *et al.*, 1996;

421   Woodson, 2018). Here, tag detection probability was high during the early stages of a flood

422   tide, and was also increased by the interaction effect between a flood tide and cooler near-

423   surface temperature, which may indicate that cold-water bores propagate up the slope

424   (Leichter *et al.*, 1996). Plankton sampling and oceanographic measurements obtained inside

425   the lagoon also indicate that increased zooplankton abundance is associated with the transfer

426   of plankton into the lagoon from the intrusion of cold water-bores created by breaking

427   internal waves (Sheehan *et al.*, 2019). The intrusion of cold water may also provide

428   metabolically advantageous feeding conditions for *M. alfredi* by reducing the energetic cost

429   of feeding activities (Lawson *et al.*, 2019)

430   In the current study, tag detection probability also increased with the interaction

431   between high-velocity near-bed cross-shore currents flowing inshore and high levels of

432   backscatter. This interaction may indicate that zooplankton is being carried from the

433   thermocline into the lagoon during a flood tide and is likely pumped back out during ebb. Due

434   to the partially enclosed morphology of the lagoon, water entering is likely to be restricted by

435   the narrow subtidal passages. Even with a low tidal amplitude, strong jet-like currents can be

436   generated (Dumas *et al.*, 2012), which may increase the density of inflowing (outflowing)

437   zooplankton approaching low tide (in the early stages of flood), as suggested by the in-water

438   observations of the current study. During these events, mobile zooplankton may actively seek

439   refuge zones to avoid predation or import into (export from) the lagoon (Pagano *et al.*, 2017).

440   Refuge zones include the thermocline and behind shallow back reefs (Leichter *et al.*, 2013),

441   where zooplankton become concentrated further, providing dense assemblages of prey for

442   *M. alfredi*. Similar theories of zooplankton retention, which are also related to tide phase,

443   have been suggested in other regions (Armstrong *et al.*, 2016; Stevens, 2016).

444   The BRT also provided some evidence of the presence of Langmuir Circulation (LC),

445   which can trap and concentrate particles in the water column (Smith, 2001). The process is

446   driven by wind and waves which produce helical vortices that appear as rotating cells that

447   rotate perpendicular to the wind direction (Smith, 2001). The interaction effect between high

448   velocity near-bed longshore currents flowing when near-surface currents were flowing in the

449   opposite direction, and high backscatter intensity could be evidence of LC cells. Alternating

450   cells rotate in opposite directions leading to areas of convergence and divergence (Talley *et*

451   *al.*, 2011). Downwelling, which increased the probability of tag detections, occurs in areas of

452   convergence where plankton, other organisms, and particles become trapped in highly

453   concentrated bands (Kingsford *et al.*, 1991; Thorpe, 2004). These bands may provide ideal

454   foraging opportunities for *M. alfredi.* As LC can persist for hours or even days (Gargett *et al.*,

455   2004), it could potentially be associated with resident events which last longer than the

456   influence of the tide (>2 hours). The characteristic surface 'slicks' which often accompany LC

457   have also been regularly observed by authors in Manta Alley, further supporting this

458   suggestion.

459   Under well-mixed conditions, LC can develop 'super-cells' which extend the full depth

460   of the water column (Gargett *et al.*, 2004). These super-cells can transport organisms and

461   partials from depths up into the water column where they become concentrated in the

462   narrow bands of the convergence zones (Gargett *et al.*, 2004; Kukulka *et al.*, 2012). Potential

463   evidence of the presence of super-cells and their positive influence on *M. alfredi* detection

464   probability is apparent with the interaction effects between high near-bed temperature near-

465   bed temperature (>28.5°C) and lower near-surface temperature (28-28.5°C), indicating a well-

466   mixed water column, warmer near-bed temperature (>28.5°C), and high backscatter, and

467   increased downward vertical velocity (downwelling) and low near-surface temperatures

468   (<28.5°C). However, high backscatter could also be caused by sediment resuspension events

469   which can be induced by LC super-cells (Gargett *et al.*, 2004). There may be evidence of the

470   effect of LC on *M. alfredi* visitation and behaviour patterns in other regions. For example, in

471   Komodo Marine Park in Indonesia, *M. alfredi* were observed feeding where there were

472   surface slicks and a high density of particles in the water column (Dewar *et al.*, 2008), which

473   is characteristic of LC convergence zones (Kingsford *et al.*, 1991). Around Lady Elliot Island

474   (LEI) in Australia, sightings of foraging individuals and increased acoustic tag detection were

475   correlated with wind speed (Jaine *et al.*, 2012; Couturier *et al.*, 2018). At LEI, *M. alfredi*

476   sightings and tag detections peaked at wind speeds around 18 km.h^{-1} (approximately 5ms^{-1}),

477   an optimal speed for the development of LC (Langmuir, 1938; Plueddemann *et al.*, 1996). At

478   LEI, sightings were also associated with cooler sea surface temperatures, with a decrease in

479   sightings and detections with increased temperature (Jaine *et al.*, 2012; Couturier *et al.*,

480   2018). Strong surface warming can lead to a breakdown of LC by disrupting the balance

481   between wave-forcing and thermal convection (density-driven circulation) (Li and Garrett,

482   1994; Min and Noh, 2004), which may reduce the density of prey, leading to a lower number

483   of sightings and tag detections of *M. alfredi.*

484   There were some limitations to the current study. For example, the position of tagged

485   *M. alfredi* in the water column and the distance the individual was from the acoustic receiver

486   and oceanographic equipment could not be established. The acoustic doppler current

487   profiler (ADCP) was also deployed on the edge of the range of the acoustic receiver.

488   Therefore, it is possible that some of the changes in the oceanographic conditions which

489   influence *M. alfredi* visitation patterns were not fully resolved here. These limitations may be

490   mitigated in future by using acoustic transmitters which also deliver distance and depth

491   information when the individual is detected. A reconfiguration of the mooring to include an

492   ADCP in line with all other sensors would also be beneficial. Future research would also

493   benefit from oceanographic monitoring within the lagoon passage and the Manta Alley

494   feeding location concurrently to help further resolve the fine-scale processes occurring at the

495   lagoon-ocean interface. Further investigation into the potential presence of LC and its

496   influence on *M. alfredi* visitation patterns at Manta Alley is also required. Research should

497   incorporate *in situ* wind directions measurements of the same spatial and temporal resolution

498   as the longshore and cross-shore current directions. These measurements should be

499   accompanied by ADCP backscatter data to detect zones of high echo intensity and periods of

500   downwelling in relation to *M. alfredi* visitation patterns, and plankton sampling to assess the

501   content of the water column during LC events.

502   Studying *M. alfredi* at Egmont Atoll provides valuable insight into how the species

503   respond to fine-scale changes in their oceanographic environment, thus improving our

504   current knowledge of *M. alfredi* foraging ecology. Evidence provided in this study suggests

505   that the species regularly take advantage of feeding opportunities which are influenced by

506   fine-scale oceanographic processes that occur close to the lagoon-ocean interface. These

507   feeding opportunities appear to occur with tidal periodicity. During a flood tide, cold-water

508   bores frequently propagate up the slope, transporting zooplankton from the thermocline into

509   the lagoon through the narrow inlet. During an ebb tide, the zooplankton then flows back out

510   of the lagoon with the highest concentrations occurring close to low tide. Mobile zooplankton

511   may become trapped and concentrated around reef structures as they attempt to avoid

512   predation by moving back into deeper water. High concentrations of zooplankton which

513   occur during these tidal phases are likely to be short-lived, occurring in pulses, providing

514   temporally limited feeding opportunities for *M. alfredi*. However, under suitable conditions,

515   for example, in the presence of LC, highly concentrated bands of zooplankton may persist for

516   hours, potentially providing extended feeding opportunities which result in *M. alfredi*

517   spending long periods of time at the location.

518

519

520

521

522

523

524   **References**

525   Alldredge, A. L. and King, J. M. (2009) 'Near-surface enrichment of zooplankton over a

526   shallow back reef: Implications for coral reef food webs', *Coral Reefs*, 28(4), pp. 895–908.

527   doi: 10.1007/s00338-009-0534-4.

528   Anderson, R. C., Adam, M. S. and Goes, J. I. (2011) 'From monsoons to mantas: Seasonal

529   distribution of *Manta alfredi* in the Maldives', *Fisheries Oceanography*, 20(2), pp. 104–113.

530   doi: 10.1111/j.1365-2419.2011.00571.x.

531   Andrzejaczek, S., Chapple, T. K., Curnick, D. J., Carlisle, A. B., Castleton, M., Jacoby, D. M. P.,

532   Schallert, R. J., Tickler, D. M. and Block, B. A. (2020) 'Individual variation in residency and

533   regional movements of reef manta rays *Mobula alfredi* in a large marine protected area',

534   *Marine Ecology Progress Series*, (639), pp. 137–153. doi: 10.3354/meps13270.

535   Armstrong, A. O., Armstrong, A. J., Jaine, F. R. A., Couturier, L. I. E., Fiora, K., Uribe-Palomino,

536   J., Weeks, S. J., Townsend, K. A., Bennett, M. B. and Richardson, A. J. (2016) 'Prey Density

537   Threshold and Tidal Influence on Reef Manta Ray Foraging at an Aggregation Site on the

538   Great Barrier Reef', *PloS one*, 11(5), p. e0153393. doi: 10.1371/journal.pone.0153393.

539   Braun, C. D., Skomal, G. B., Thorrold, S. R. and Berumen, M. L. (2014) 'Diving behavior of the

540   reef manta ray links coral reefs with adjacent deep pelagic habitats', *PLoS ONE*, 9(2), pp. 1–

541   8. doi: 10.1371/journal.pone.0088170.

542   Campbell, H. A., Watts, M. E., Dwyer, R. G. and Franklin, C. E. (2012) 'V-Track: Software for

543   analysing and visualising animal movement from acoustic telemetry detections', *Marine and*

544   *Freshwater Research*, 63(9), pp. 815–820. doi: 10.1071/MF12194.

545   Cerutti-Pereyra, F., Thums, M., Austin, C. M., Bradshaw, C. J. A., Stevens, J. D., Babcock, R.

546   C., Pillans, R. D. and Meekan, M. G. (2014) 'Restricted movements of juvenile rays in the

547   lagoon of Ningaloo Reef, Western Australia - evidence for the existence of a nursery',

548   *Environmental Biology of Fishes*, 97(4), pp. 371–383. doi: 10.1007/s10641-013-0158-y.

549   Colin, B., Clifford, S., Wu, P., Rathmanner, S. and Mengersen, K. (2017) 'Using Boosted

550   Regression Trees and Remotely Sensed Data to Drive Decision-Making', *Open Journal of*

551   *Statistics*, 07(05), pp. 859–875. doi: 10.4236/ojs.2017.75061.

552   Côté, I. M. (2000) 'Evolution and ecology of cleaning symbiosis in the sea', in Gibson, R. N.

553   and Barnes, M. (eds) *Oceanography and Marine Biology: An Annual Review*. London: Taylor

554   & Francis, pp. 311–355.

555   Couturier, L. I. E., Marshall, A. D., Jaine, F. R. A., Kashiwagi, T., Pierce, S. J., Townsend, K. A.,

556   Weeks, S. J., Bennett, M. B. and Richardson, A. J. (2012) 'Biology, ecology and conservation

557   of the Mobulidae', *Journal of Fish Biology*, 80, pp. 1075–1119. doi:10.1111/j.1095-

558   8649.2012.03264.x.

559   Couturier, L. I. E., Newman, P., Jaine, F. R. A., Bennett, M. B., Venables, W. N., Cagua, E. F.,

560   Townsend, K. A., Weeks, S. J. and Richardson, A. J. (2018) 'Variation in occupancy and

561   habitat use of *Mobula alfredi* at a major aggregation site', *Marine Ecology Progress Series*,

562   599(July), pp. 125–145. doi: 10.3354/meps12610.

563   Couturier, L. I. E., Rohner, C. A., Richardson, A. J., Marshall, A. D., Jaine, F. R. A., Bennett, M.

564   B., Townsend, K. A., Weeks, S. J. and Nichols, P. D. (2013) 'Stable Isotope and Signature Fatty

565   Acid Analyses Suggest Reef Manta Rays Feed on Demersal Zooplankton', *PLoS ONE*, 8(10).

566   doi: 10.1371/journal.pone.0077152.

567   Daly, R., Smale, M. J., Cowley, P. D. and Froneman, P. W. (2014) 'Residency patterns and

568　　migration dynamics of adult bull sharks (*Carcharhinus leucas*) on the east coast of Southern

569　　Africa', *PLoS ONE*, 9(10). doi: 10.1371/journal.pone.0109357.

570　　Deakos, M. H. (2011) 'The reproductive ecology of resident manta rays (*Manta alfredi*) off

571　　Maui, Hawaii, with an emphasis on body size', *Environmental Biology of Fishes*, 94(2), pp.

572　　443–456. doi: 10.1007/s10641-011-9953-5.

573　　Dedman, S., Officer, R., Brophy, D., Clarke, M. and Reid, D. G. (2017) 'Advanced Spatial

574　　Modeling to Inform Management of Data-Poor Juvenile and Adult Female Rays', *Fishes*, 2(3),

575　　p. 12. doi: 10.3390/fishes2030012.

576　　Derville, S., Constantine, R., Baker, C., Oremus, M. and Torres, L. (2016) 'Environmental

577　　correlates of nearshore habitat distribution by the Critically Endangered Maūi dolphin',

578　　*Marine Ecology Progress Series*, 551(May 2015), pp. 261–275. doi: 10.3354/meps11736.

579　　Dewar, H., Mous, P., Domeier, M., Muljadi, A., Pet, J. and Whitty, J. (2008) 'Movements and

580　　site fidelity of the giant manta ray, *Manta birostris,* in the Komodo Marine Park, Indonesia',

581　　*Marine Biology*, 155(2), pp. 121–133. doi: 10.1007/s00227-008-0988-x.

582　　Dulvy, N. K., Pardo, S. A., Simpfendorfer, C. A. and Carlson, J. K. (2014) 'Diagnosing the

583　　dangerous demography of manta rays using life history theory', *PeerJ*, 2, p. e400. doi:

584　　10.7717/peerj.400.

585　　Dumas, F., Le Gendre, R., Thomas, Y. and Andréfouët, S. (2012) 'Tidal flushing and wind

586　　driven circulation of Ahe atoll lagoon (Tuamotu Archipelago, French Polynesia) from in situ

587　　observations and numerical modelling', *Marine Pollution Bulletin*. Elsevier Ltd, 65(10–12),

588　　pp. 425–440. doi: 10.1016/j.marpolbul.2012.05.041.

589　　Elith, J. and Leathwick, J. (2017) 'Boosted Regression Trees for ecological modelling', pp. 1–

590   22. doi: 10.1890/0012-9658(2007)88[243:BTFEMA]2.0.CO;2.

591   Elith, J., Leathwick, J. R. and Hastie, T. (2008) 'A working guide to boosted regression trees',

592   *Journal of Animal Ecology*, 77 (4), pp. 802–813. doi: 10.1111/j.1365-2656.2008.01390.x.

593   Friedman, J. H. (2001) 'Greedy Function Approximation: A Gradient Boosting Machine', *The*

594   *Annals of Statistics*, 29 (5), pp. 1189–1232. doi:10.1214/aos/1013203451.

595   Froeschke, J., Stunz, G. W. and Wildhaber, M. L. (2010) 'Environmental influences on the

596   occurrence of coastal sharks in estuarine waters', *Marine Ecology Progress Series*, 407, pp.

597   279–292. doi: 10.3354/meps08546.

598   Gargett, A., Wells, J., Tejada-Martínez, A. E. and Grosch, C. E. (2004) 'Langmuir supercells: A

599   mechanism for sediment resuspension and transport in shallow seas', *Science*, 306 (5703),

600   pp. 1925–1928. doi: 10.1126/science.1100849.

601   Genin, A., Jaffe, J. S., Reef, R., Richter, C. and Franks, P. J. S. (2005) 'Swimming against the

602   flow: A mechanism of zooplankton aggregation', *Science*, 308(5723), pp. 860–862. doi:

603   10.1126/science.1107834.

604   Harris, J. L. (2019) *Habitat use of reef manta rays, Mobula afredi, in the Chagos Archipelago*

605   *and the effectiveness of the region's marine protected area for this vulnerable species*. MRes

606   Thesis. University of Plymouth, Plymouth.

607   Harris, J. L., McGregor, P., Oates, Y. and Stevens, G. (2020) 'Gone with the wind: seasonal

608   distribution and habitat use by the reef manta ray (*Mobula alfredi*) in the Maldives,

609   implications for conservation', *Aquatic Conservation: Marine and Freshwater Ecosystems*,

610   30, pp. 30:1649–1664. doi: 10.1002/aqc.3350

611   Hastie, T., Tibshirani, R. and Friedman, J. (2009) *The Elements of Statistical Learning The*

612   *Elements of Statistical Learning Data Mining, Inference, and Prediction*. 2nd edn. New York:

613   Springer-Verlag.

614   Hijmans, Phillips, S., Leathwick, J. R. and Elith, J. (2017) *Species Distribution Modeling*

615   *Version Dismo package for R, version 1.1-4*. doi: 10.1016/j.jhydrol.2011.07.022.

616   Hosegood, P. J., Nimmo-Smith, W. A. M., Proud, R., Adams, K. and Brierley, A. S. (2019)

617   'Internal lee waves and baroclinic bores over a tropical seamount shark "hot-spot"',

618   *Progress in Oceanography*. Elsevier, 172, pp. 34–50. doi: 10.1016/j.pocean.2019.01.010.

619   Hosegood, J., Humble, E., Ogden, R., de Bruyn, M., Creer, S., Stevens, G. M.W., Abudaya, M.,

620   Bassos-Hull, K., Bonfil, R., Fernando, D., Foote, A. D., Hipperson, H., Jabado, R. W., Kaden, J.,

621   Moazzam, M., Peel, L.R.., Pollett, S., Ponzo, A., Poortvliet, M., Salah, J., Senn, H., Stewart,

622   J.D., Wintner, S., Carvalho, G. (2020) 'Phylogenomics and species delimitation for effective

623   conservation of manta and devil rays', *Molecular Ecology*, 29(24), pp. 4783–4796. doi:

624   10.1111/mec.15683.

625   Hosmer, D. W. and Lemeshow, S. (2000) *Applied Logistic Regression*. Toronto: John Wiley &

626   Sons Inc. doi: 10.1074/jbc.272.33.20373.

627   Jaine, F. R. A., Couturier, L. I. E., Weeks, S. J., Townsend, Kathy A. Bennett, M. B., Fiora, K.

628   and Richardson, A. J. (2012) 'When Giants Turn Up: Sighting Trends, Environmental

629   Influences and Habitat Use of the Manta Ray *Manta alfredi* at a Coral Reef', *PLoS ONE*, 7(10),

630   p. e46170. doi: 10.1371/journal.pone.0046170.

631   Jaine, F. R. A., Rohner, C. A., Weeks, S. J., Couturier, L. I. E., Bennett, M. B., Townsend, K. A.

632   and Richardson, A. J. (2014) 'Movements and habitat use of reef manta rays off eastern

633   Australia: Offshore excursions, deep diving and eddy affinity revealed by satellite telemetry',

634   *Marine Ecology Progress Series*, 510 (September), pp. 73–86. doi: 10.3354/meps10910.

635   Jouffray, J., Wedding, L. M., Norstro, A. V, Donovan, M. K., Williams, G. J., Crowder, L. B.,

636   Erickson, A. L., Friedlander, A. M., Graham, N. A. J., Gove, J. M., Kappel, C. V, Kittinger, J. N.,

637   Lecky, J. and Oleson, K. L. L. (2019) 'Parsing human and biophysical drivers of coral reef

638   regimes', *Preceedings B*, 268, p. 20182544. doi: 10.1098/rspb.2018.2544.

639   Kessel, S. T., Elamin, N. A., Yurkowski, D. J., Chekchak, T., Walter, R. P., Klaus, R., Hill, G. and

640   Hussey, N. E. (2017) 'Conservation of reef manta rays (*Manta alfredi*) in a UNESCO World

641   Heritage Site: Large-scale island development or sustainable tourism?', *PLoS ONE*, 12(10),

642   pp. 1–16. doi: 10.1371/journal.pone.0185419.

643   Kingsford, M. J., Wolanski, E. and Choat, J. H. (1991) 'Influence of tidally induced fronts and

644   Langmuir circulations on distribution and movements of presettlement fishes around a coral

645   reef', *Marine Biology*, 109, pp. 167–180. doi: 10.1007/BF01320244.

646   Kuiter, R. H. (2014) *Fishes of the Maldives – Indian Ocean: Applicable to Central and Western*

647   *Indian Ocean: East Africa, Seychelles, Mauritius, Reunion, Madagascar, Sri Lanka, Chagos,*

648   *Laccadives, Cocos Keeling Islands*. Cairns, Australia: Atoll Editions.

649   Kukulka, T., Plueddemann, A. J. and Sullivan, P. P. (2012) 'Nonlocal transport due to

650   Langmuir circulation in a coastal ocean', *Journal of Geophysical Research: Oceans*, 117(12),

651   pp. 1–17. doi: 10.1029/2012JC008340.

652   Langmuir, I. (1938) 'Surface motion of water induced by wind', *Science*, 87, pp. 119–123.

653   doi: 10.1126/science.87.2250.119.

654   Lawson, J. M., Fordham, S. V., O'Malley, M. P., Davidson, L. N. K., Walls, R. H. L., Heupel, M.

655   R., Stevens, G., Fernando, D., Budziak, A., Simpfendorfer, C. A., Ender, I., Francis, M. P.,

656   Notarbartolo di Sciara, G. and Dulvy, N. K. (2017) 'Sympathy for the devil: a conservation

657   strategy for devil and manta rays', *PeerJ*, 5, p. e3027. doi: 10.7717/peerj.3027.

658   Lawson, C. L., Halsey, L. G., Hays, G. C., Dudgeon, C. L., Payne, N. L., Bennett, M. B., White, C.

659   R., Richardson, A. J. (2019) 'Powering Ocean Giants: The Energetics of Shark and Ray

660   Megafauna', *Trends in Ecology and Evolution*. Elsevier Inc., 34(11), pp. 1009–1021. doi:

661   10.1016/j.tree.2019.07.001.

662   Lea, J. S. E. (2017) *Migratory behaviour and spatial dynamics of large sharks and their*

663   *conservation implications*. PhD Thesis. University of Plymouth, Plymouth.

664   Leichter, J. J., Alldredge, A. L., Bernardi, G., Brooks, A. J., Carlson, C. A., Carpenter, R. C.,

665   Edmunds, P. J., Fewings, M. R., Hanson, K. M., Hench, J. L., Holbrook, S. J., Nelson, C. E.,

666   Schmitt, R. J., Toonen, R. J., Washburn, L. and Wyatt, A. S. J. (2013) 'Biological and physical

667   interactions on a tropical island coral reef: Transport and retention processes on moorea,

668   French Polynesia', *Oceanography*, 26(3), pp. 52–63. doi: 10.5670/oceanog.2013.45.

669   Leichter, J. J., Wing, S. R., Miller, S. L. and Denny, M. W. (1996) 'Pulsed delivery of

670   subthermocline water to Conch Reef (Florida Keys) by internal tidal bores', *Limnology and*

671   *Oceanography*, 41(7), pp. 1490–1501. doi: 10.4319/lo.1996.41.7.1490.

672   Li, M. and Garrett, C. (1994) 'Is Langmuir Circulation driven by surface waves or surface

673   cooling?', *Journal of Physical Oceanography*, 25, pp. 64–76. doi: 10.1175/1520-

674   0485(1995)025<0064:ILCDBS>2.0.CO;2

675   Marshall, A., Barreto, R., Carlson, J., Fernando, D., Fordham, S., Francis, M. P., Herman, K.,

676   Jabado, R. W., Liu, K. M., Pacoureau, N., Rigby, C. L., Romanov, E. and Sherley, R. B. (2019)

677   '*Mobula alfredi*', *The IUCN Red List of Threatened Species*, e.T195459A, p. 19.

678   Marshall, A. D., Compagno, L. J. V and Bennett, M. B. (2009) 'Redescription Of The Genus

679   Manta With Resurrection Of *Manta Alfredi* (Krefft, 1868) (Chondrichthyes; Myliobatoidei;

680   Mobulidae)', *Zootaxa*, 2301 (December), pp. 1–28. doi: 10.5281/zenodo.191734.

681   Marshall, A. D. and Pierce, S. J. (2012) 'The use and abuse of photographic identification in

682   sharks and rays', *Journal of Fish Biology*, 80 (5), pp. 1361–1379. doi: 10.1111/j.1095-

683   8649.2012.03244.x.

684   McCauley, D. J., DeSalles, P. A., Young, H. S., Papastamatiou, Y. P., Caselle, J. E., Deakos, M.

685   H., Gardner, J. P. A., Garton, D. W., Collen, J. D. and Micheli, F. (2014) 'Reliance of mobile

686   species on sensitive habitats: A case study of manta rays (*Manta alfredi*) and lagoons',

687   *Marine Biology*, 161 (9), pp. 1987–1998. doi: 10.1007/s00227-014-2478-7.

688   McManus, M., Cheriton, O., Greenlaw, C., Donaghay, P., Storlazzi, C., Holliday, D. and Drake,

689   P. (2005) 'Effects of physical processes on structure and transport of thin zooplankton layers

690   in the coastal ocean', *Marine Ecology Progress Series*, 301, pp. 199–215. doi:

691   10.3354/meps301199.

692   Min, H. S. and Noh, Y. (2004) 'Influence of the surface heating on Langmuir circulation',

693   *Journal of Physical Oceanography*, 34(12), pp. 2630–2641. doi: 10.1175/JPOJPO-2654.1.

694   Morel, A., Claustre, H. and Gentili, B. (2010) 'The most oligotrophic subtropical zones of the

695   global ocean: Similarities and differences in terms of chlorophyll and yellow substance',

696   *Biogeosciences*, 7(10), pp. 3139–3151. doi: 10.5194/bg-7-3139-2010.

697   Murray, A., Garrud, E., Ender, I., Lee-Brooks, K., Atkins, R., Lynam, R., Arnold, K., Roberts, C.,

698   Hawkins, J. and Stevens, G. (2019) 'Protecting the million-dollar mantas; creating an

699   evidence-based code of conduct for manta ray tourism interactions', *Journal of Ecotourism*,

700   19(2), pp. 132–147. doi: 10.1080/14724049.2019.1659802.

701   Nalesso, E., Hearn, A., Sosa-Nishizaki, O., Steiner, T., Antoniou, A., Reid, A., Bessudo, S.,

702   Soler, G., Peter Klimley, A., Lara, F., Ketchum, J. T. and Arauz, R. (2019) 'Movements of

703   scalloped hammerhead sharks (*Sphyrna lewini*) at Cocos Island, Costa Rica and between

704   oceanic islands in the Eastern Tropical Pacific', *PLoS ONE*, 14(3), pp. 1–16. doi:

705   10.1371/journal.pone.0213741.

706   Nieto, K. and Mélin, F. (2017) 'Variability of chlorophyll-a concentration in the Gulf of

707   Guinea and its relation to physical oceanographic variables', *Progress in Oceanography*, 151,

708   pp. 97–115. doi: 10.1016/j.pocean.2016.11.009.

709   Nøttestad, L., Giske, J., Holst, J. C. and Huse, G. (1999) 'A length-based hypothesis for

710   feeding migrations in pelagic fish', *Canadian Journal of Fisheries and Aquatic Sciences*,

711   56(S1), pp. 26–34. doi: 10.1139/cjfas-56-S1-2.

712   O'Malley, M. p., Townsend, K. A., Hilton, P., Heinrichs, S. and Stewart, J. D. (2017)

713   'Characterization of the trade in manta and devil ray gill plates in China and South-east Asia

714   through trader surveys', *Aquatic Conservation: Marine and Freshwater Ecosystems*, 27(2),

715   pp. 394–413. doi: 10.1002/aqc.2670.

716   O'Shea, O. R., Kingsford, M. J. and Seymour, J. (2010) 'Tide-related periodicity of manta rays

717   and sharks to cleaning stations on a coral reef', *Marine and Freshwater Research*, 61, pp.

718   65–73. doi: 10.1071/MF08301.

719   Pagano, M., Rodier, M., Guillaumot, C., Thomas, Y., Henry, K. and Andréfouët, S. (2017)

720   'Ocean-lagoon water and plankton exchanges in a semi-closed pearl farming atoll lagoon

721   (Ahe, Tuamotu archipelago, French Polynesia)', *Estuarine, Coastal and Shelf Science*,

Ecology and Evolution

722   191(April), pp. 60–73. doi: 10.1016/j.ecss.2017.04.017.

723   Paig-Tran, E. W. M., Kleinteich, T. and Summers, A. P. (2013) 'The filter pads and filtration

724   mechanisms of the devil rays: Variation at macro and microscopic scales', *Journal of*

725   *Morphology*, 274(9), pp. 1026–1043. doi: 10.1002/jmor.20160.

726   Peel, L. R., Daly, R., Keating Daly, C. A., Stevens, G. M. W., Collin, S. P. and Meekan, M. G.

727   (2019a) 'Stable isotope analyses reveal unique trophic role of reef manta rays (*Mobula*

728   *alfred*) at a remote coral reef', *Royal Society Open Science*, 6(9), p. 190599. doi:

729   10.1098/rsos.190599.

730   Peel, L. R., Stevens, G., Daly, R., Daly, C., Lea, J., Clarke, C., Collin, S. and Meekan, M. (2019b)

731   'Movement and residency patterns of reef manta rays *Mobula alfredi* in the Amirante

732   Islands, Seychelles', *Marine Ecology Progress Series*, 621, pp. 169–184. doi:

733   10.3354/meps12995.

734   Perryman, R. J. Y., Venables, S. K., Tapilatu, R. F., Marshall, A.D., Brown, C., Franks, D. W.

735   (2019) 'Social preferences and network structure in a population of reef manta rays',

736   *Behavioral Ecology and Sociobiology*. Behavioral Ecology and Sociobiology, 73(8). doi:

737   10.1007/s00265-019-2720-x.

738   Pinsky, M. L. and Byler, D. (2015) 'Fishing , fast growth and climate variability increase the

739   risk of collapse', *Proceedings B*, 282, p. 20151053. doi: 10.1098/rspb.2015.1053.

740   Plueddemann, A. J., Smith, J. A., Farmer, D. M., Weller, R. A., Crawford, W. R., Pinkel, R.,

741   Vagle, S. and Gnanadesikan, A. (1996) 'Structure and variability of Langmuir circulation

742   during the Surface Waves Processes Program', *Journal of Geophysical Research C: Oceans*,

743   101(C2), pp. 3525–3543. doi: 10.1029/95JC03282.

744   R Core Team (2018) *R: A language and environment for statistical computing. R Foundation*

745   *for Statistical Computing*. Vienna. Available at: https://www.r-project.org/.(Accessed 15th

746   December 2019).

747   Readman, J. W., Deluna, F., Ebinghaus, R., Guzman, A., Price, A. R. G., Emily, E., Sheppard, A.

748   L. S., Sleight, V. A., Thompson, R. C., Tonkin, A., Wright, R. J. and Sheppard, C. R. C. (2013)

749   'Contaminants, Pollution and Potential Anthropogenic Impacts in Chagos/BIOT', in

750   Sheppard, C. (ed.) *Coral reefs of the United Kingdom overseas territories*. 1st edn. Dordrecht:

751   Springer Netherlands, pp. 51-1468-51–1468. doi: 10.5860/choice.51-1468.

752   Richardson, A. (2008) 'In hot water: zooplankton and climate change', *ICES Journal of*

753   *Marine Science*, 65(279–295), pp. 279–295. doi: 10. 1093/icesjms/fsn028.

754   Rohner, C. A., Flam, A. L., Pierce, S. J. and Marshall, A. D. (2017) 'Steep declines in sightings

755   of manta rays and devilrays (Mobulidae) in southern Mozambique', *PeerJ Preprints* ,

756   5:e3051v1. doi: 10.7287/peerj.preprints.3051v1

757   Roxy, M. K., Modi, A., Murtugudde, R., Valsala, V., Kumar, S. P., Ravichandran, M., Vichi, M.,

758   Lévy, M., Roxy, M. K., Modi, A., Murtugudde, R., Valsala, V. and Panickal, S. (2016) 'A

759   reduction in marine primary productivity driven by rapid warming over the tropical Indian

760   Ocean', *Geophysical Research Letters*, 43, pp. 826–833. doi: 10.1002/2015GL066979.

761   Setyawan, E., Sianipar, A. B., Erdmann, M. V., Fischer, A. M., Haddy, J. A., Beale, C. S., Lewis,

762   S. A. and Mambrasar, R. (2018) 'Site fidelity and movement patterns of reef manta rays

763   (*Mobula alfredi*: Mobulidae) using passive acoustic telemetry in northern Raja Ampat,

764   Indonesia', *Nature Conservation Research*, 3(4), pp. 1-15, doi: 10.24189/ncr.2018.043.

765   Shanks, A. L., Morgan, S. G., MacMahan, J., Reniers, A. J. H. M., Reniers, M., Brown, J.,

766   Fujimura, A. and Griesemer, C. (2014) 'Onshore transport of plankton by internal tides and

767   upwelling-relaxation events', *Marine Ecology Progress Series*, 502, pp. 39–51. doi:

768   10.3354/meps10717.

769   Sheehan, E. V, Hosegood, P., Game, C. A., Attrill, M. J., Tickler, D., Wootton, M., Johns, D. G.

770   and Meeuwig, J. J. (2019) 'The Effect of Deep Oceanic Flushing on Water Properties and

771   Ecosystem Functioning Within Atolls in the British Indian Ocean Territory', 6 (August), pp. 1–

772   13. doi: 10.3389/fmars.2019.00512.

773   Sheppard *et al.* (2012) 'Reefs and islands of the Chagos Archipelago, Indian Ocean: Why it is

774   the world's largest no-take marine protected area', *Aquatic Conservation: Marine and*

775   *Freshwater Ecosystems*, 22 (2), pp. 232–261. doi: 10.1002/aqc.1248.

776   Simpfendorfer, C. A., Huveneers, C., Steckenreuter, A., Tattersall, K., Hoenner, X., Harcourt,

777   R. and Heupel, M. R. (2015) 'Ghosts in the data: False detections in VEMCO pulse position

778   modulation acoustic telemetry monitoring equipment', *Animal Biotelemetry*. BioMed

779   Central, 3(1), pp. 1–10. doi: 10.1186/s40317-015-0094-z.

780   Smith, J. A. (2001) 'Observations and Theories of Langmuir Circulation: A Story of Mixing',

781   *Fluid Mechanics and the Environment: Dynamical Approaches*. Edited by Lumley, J.L.

782   Springer Berlin Heidelberg, 566, pp. 295–314. doi: 10.1007/3-540-44512-9_16.

783   Stevens, G. M. W. (2016) *Conservation and Population Ecology of Manta Rays in the*

784   *Maldives*. PhD Thesis. University of York, Heslington.

785   Stevens, G. M. W., Hawkins, J. P. and Roberts, C. M. (2018) 'Courtship and mating behaviour

786   of manta rays *Mobula alfredi* and *M. birostris* in the Maldives', *Journal of Fish Biology*, 93(2),

787   pp. 344–359. doi: 10.1111/jfb.13768.

788   Stevick, P. T., Incze, L. S., Kraus, S. D., Rosen, S., Wolff, N. and Baukus, A. (2008) 'Trophic

789   relationships and oceanography on and around a small offshore bank', *Marine Ecology*

790   *Progress Series*, 363, pp. 15–28. doi: 10.3354/meps07475.

791   Stewart, J. D., Nuttall, M., Hickerson, E. L. and Johnston, M. A. (2018) 'Important juvenile

792   manta ray habitat at Flower Garden Banks National Marine Sanctuary in the northwestern

793   Gulf of Mexico', *Marine Biology*. Springer Berlin Heidelberg, 165(7). doi: 10.1007/s00227-

794   018-3364-5.

795   Talley, L. D., Pickard, G. L., Emery, W. J. and Swift, J. H. (2011) 'Dynamical Processes for

796   Descriptive Ocean Circulation', *Descriptive Physical Oceanography*, pp. 1–72. doi:

797   10.1016/b978-0-7506-4552-2.10019-8.

798   Thorpe, S. A. (2004) 'Langmuir Circulation', *Annual Review of Fluid Mechanics*, 36(1), pp. 55–

799   79. doi: 10.1146/annurev.fluid.36.052203.071431.

800   Venables, S., Mcgregor, F., Brain, L. and Van Keulen, M. (2016) 'Manta ray tourism

801   management, precautionary strategies for a growing industry: A case study from the

802   Ningaloo Marine Park, Western Australia', *Pacific Conservation Biology*, 22(4), pp. 295–300.

803   doi: 10.1071/PC16003.

804   White, W. T., Corrigan, S., Yang, L., Henderson, A. C., Bazinet, A. L., Swofford, D. L. and

805   Naylor, G. J. P. (2017) 'Phylogeny of the manta and devilrays (Chondrichthyes: mobulidae),

806   with an updated taxonomic arrangement for the family', *Zoological Journal of the Linnean*

807   *Society*, 182(1), pp. 50–75. doi: 10.1093/zoolinnean/zlx018.

808   Woodroffe, C. D. and Biribo, N. (2011) 'Atolls', in David Hopley (ed.) *Encyclopedia of Modern*

809   *Coral Reefs: Structure, Form and Process*. Dordrecht: Springer Netherlands, pp. 51–70.

810   Woodson, C. B. (2018) 'The fate and impact of internal waves in nearshore ecosystems',

811   *Annual Review of Marine Science*, 10(August 2017), pp. 421–441. doi: 10.1146/annurev-

812   marine-121916-063619.

813

814

815

816

817

818

819

820

821

822

823

824

825

826

827

828

829

830

831

832 **Table 1**: Description of the predictor variables used in boosted regression trees analysis of tagged *Mobula alfredi*

833 occurrence at Manta Alley. All predictors are in 5-min means unless otherwise specified. All distances are metres

834 above the seabed. Mean values show the value at which the predictor is held for partial dependency and

835 interaction plots.

Predictor No.	Predictor	Unit	Mean	Description
1	Temp 2 m	°C	27.7	Temperature 2 m above the bed (depth 64.1 m)
2	Temp 50 m	°C	29.1	Temperature 50 m above the bed (depth 13.4 m)
3	Backscatter	dB	46.1	Depth-mean linearly interpolated into 5-min bins
4	Cross-shore (v) 48.5 m	ms^{-1}	-0.007	Surface current 48.5 m above the bed (depth 17.6 m) flowing 27° (-ve) and 207° (+ve) relative to N
5	Cross-shore (v) 8.5 m	ms^{-1}	-0.016	Near bed current 8.5 m above the bed (depth 57.6 m) flowing 27° (-ve) and 207° (+ve) relative to N
6	Longshore (u) 48.5 m	ms^{-1}	-0.095	Near surface current 48.5 m above the bed (depth 17.6 m) flowing 117° (-ve) and 297° (+ve) relative to N
7	Longshore (u) 8.5 m	ms^{-1}	-0.078	Near bed current 8.5 m above the bed (depth 57.6

				m) flowing 117° (-ve) and 297° (+ve) relative to N
8	Vertical velocity	ms^{-1}	0.002	Upward (+ve) and downward (-ve) current flow.
9	Time to high tide	0.083 h	0.014	Time relative to high tide in steps of 5-min (0.083h) with high tide zero, negative values before (flood) and positive values after (ebb).

836

837

838 **Table 2**: Summary of *Mobula alfredi* acoustic tag deployments (n=19), tracking, detections and Residency Index (RI) for Egmont Atoll. Status refers to the known status of

839 tags at the time of last detection data download (17th March 2020).

Manta ID	Sex	Maturity status	Tag ID	Deployment Date	Deployment Location	Lat	Long	Last Detection	Total No. of Detection	Tracking Days	Detection Days	Residency Index (RI%)	Status
CG-MA-0035	F	Sub-adult	18890	20/11/2019	Ile Sipaille	-6.67	71.32	13/03/2020	1159	115	92	80	ACTIVE
CG-MA-0046	F	Adult	18892	25/11/2019	Ile Tattamucca	-6.69	71.38	10/03/2020	846	107	61	57	ACTIVE
CG-MA-0070	F	Adult	18891	01/12/2019	Ile Lubine	-6.67	71.32	17/03/2020	1059	108	46	43	ACTIVE
CG-MA-0088	M	Juvenile	18897	28/11/2019	Ile Lubine	-6.67	71.32	15/03/2020	907	109	43	40	ACTIVE
CG-MA-0094	F	Sub-adult	18894	30/11/2019	Ile Sipaillle	-6.66	71.31	13/03/2020	1116	105	67	64	ACTIVE
CG-MA-0112	M	Juvenile	18893	01/12/2019	Ile Lubine/Sipaillle	-6.66	71.31	13/03/2020	1129	104	49	47	ACTIVE
CG-MA-0117	F	Sub-adult	18887	20/11/2019	Ile Lubine	-6.67	71.32	13/03/2020	718	115	50	44	ACTIVE
CG-MA-0118	M	Juvenile	18900	19/11/2019	Ile Sipalle	-6.66	71.31	11/03/2020	678	114	41	36	ACTIVE
CG-MA-0119	F	Juvenile	18901	19/11/2019	Ile Sipalle	-6.67	71.32	13/03/2020	801	116	54	47	ACTIVE
CG-MA-0120	F	Adult	18902	19/11/2019	Ile Sipalle	-6.67	71.32	21/11/2019	15	3	2	76	UNKNOWN
CG-MA-0121	M	Juvenile	18903	19/11/2019	Ile Sipalle	-6.67	71.32	13/03/2020	1770	116	84	73	ACTIVE
CG-MA-0124	M	Adult	18885	20/11/2019	Ile Lubine	-6.67	71.32	12/03/2020	559	114	44	39	ACTIVE
CG-MA-0125	M	Juvenile	18895	20/11/2019	North IDR Cleaning St	-6.64	71.32	14/03/2020	1272	116	60	52	ACTIVE
CG-MA-0139	F	Adult	18899	25/11/2019	Ile Tattamucca	-6.69	71.38	15/03/2020	763	112	73	66	ACTIVE
CG-MA-0140	M	Juvenile	18898	30/11/2019	North IDR Cleaning St	-6.64	71.32	13/03/2020	711	105	25	24	ACTIVE

CG-MA-0141	F	Adult	18889	28/11/2019	Ile Lubine	-6.67	71.32	20/01/2020	411	54	31	58	UNKNOWN
CG-MA-0142	F	Sub-adult	18884	02/12/2019	Ile Tattamucca	-6.70	71.40	15/03/2020	1216	105	59	56	ACTIVE
CG-MA-0151	M	Adult	18896	01/12/2019	Ile Lubine	-6.68	71.33	12/03/2020	794	103	62	60	ACTIVE
CG-MA-0161	M	Adult	18888	02/12/2019	Ile Carre Pate	-6.68	71.35	27/12/2019	41	26	7	27	UNKNOWN

840

841

842

843

844

845

846

847

848

849

850

851   **Table 3**: Summary of acoustic receiver deployment locations, recording times and resident event durations.

Location	Deployed	Lat	Long	Depth (m)	Height above seabed (m)	No. days recording	No. *M. alfredi*	Mean resident event (min±SD)	Max resident event (mins)
Ile Sipaille	19/11/2019	71.32	-6.67	14.6	1.5	116	19	15±26	200
Ile Sudest	01/12/2019	71.40	-6.70	15	1.8	104	11	5±10	56
Manta Alley	30/11/2019	71.35	-6.64	70	48	109	18	27±51	489
North IdR Cleaning Station	19/11/2019	71.32	-6.64	13.6	1.6	116	17	19±36	294
South Manta Alley	30/11/2019	71.39	-6.67	14.2	1.8	105	18	16±26	133

852

853

854

855

856

857   **Table 4**: Pairwise interactions between predictor variables with all other variables held to their respective mean (Table 1). Higher interaction size values indicate a more

858   substantial interaction effect; near zero indicates negligible interactions. All interactions were significant ($p<0.01$). The suggested influence of the interaction on the

859   probability of detections is described along with the maximum detection probability estimated for each interaction.

Plot	Predictor 1	Predictor 2	Interaction size	Nature of interaction increasing tag detection probability	Max detection probability (%)
S2a	Temp 50 m	Vertical velocity	768.77	Warmer near-surface temperature and increased upward vertical velocity.	90
S2b	Temp 50 m	Temp 2 m	741.86	Cooler near-bed temperature and increased near-surface temperature indicating the water column is stratified. Warmer near-bed temperature (>28.5°C) with similar near-surface temperature (28-28.5°C)	92
S2c	Cross-shore (v) 8.5 m	Backscatter	427.88	Near-bed longshore currents flowing at velocity of >0.15ms^{-1} (+ve, flowing into the lagoon) and high backscatter intensity (>55).	85

43

S2d	Temp 2 m	Backscatter	405.69	Warmer near-bed temperature (>29.5°C) and high backscatter intensity (>55).	98
S2e	Longshore (u) 8.5 m	Time to high tide	165.86	During the early stages of flood with increasing near-bed longshore current velocity (+ve, flowing from North IdR Cleaning Station towards South Manta Alley) flowing from the	86
S2f	Longshore (u) 48.5 m	Time to high tide	124.66	During the early stages of flood with moderate velocity (approximately 0.3-0.4 ms^{-1}) longshore near-surface current (+ve, flowing from North IdR Cleaning Station towards South Manta Alley)	66
S2g	Temp 50 m (53%)	Time to high tide	182.1	During the early stages of flood with cooler near-surface temperature (<29°C) and during ebb close to low tide with warmer near-surface temperature (>29.5°C).	59
S2h	Longshore (v) 8.5 m	Backscatter	100.63	Longshore near-bed currents flowing at moderate to the maximum speed observed (-0.66 ms^{-1}) from South Manta Alley towards North IdR Cleaning Station, and high backscatter intensity (>55).	73

861 **Figure 1:** The Central Indian Ocean with Chagos Archipelago; British Indian Ocean Territory

862 indicated within the red box (left inset). The Chagos Archipelago with Egmont Atoll indicated

863 within the red box (left). Egmont Atoll and the location of the oceanographic and acoustic

864 receiver mooring in Manta Alley (red and yellow dots) and four acoustic receivers (green dots)

865 (top right). Bathymetric view of Manta Alley obtained via multibeam survey (Robinson and

866 Hosegood *et al.*, unpublished data) showing the location of the moorings (bottom right).

867 Bottom right legend showing instrument configurations of the long thermistor string (red

868 dot/pin) and subsurface ADCP moorings (yellow dot/pin) deployed 182 m apart anchored at

869 a depth of 66 m. Z is the height above the seabed.

870 **Figure 2**: Reef manta rays (*Mobula alfredi*) engaged in feeding activities at the Manta Alley

871 feeding aggregation site in north Egmont Atoll. Photo by Simon Hilbourne, Manta Trust.

872 **Figure 3**: Original current u and v components (yellow dashed lines) and after clockwise

873 rotation 117° relative to north (white lines). Arrows on the white lines show the direction of

874 longshore u (LS U-ve and LS U+ve) and cross-shore v (CS V-ve and CS V+ve). Showing mooring

875 locations: long thermistor string (red dot) and subsurface ADCP moorings (yellow dot).

876 **Figure 4**: Percentage of detections at each site.

877 **Figure 5:** Percentage distribution of detections by hour of the day at Egmont Atoll for all

878 tagged *M. alfredi* (left), adults only (middle) and juveniles only (right).

879 **Figure 6**: Resident events at each site showing location (by colour) and time at the location

880 (by size).

881 **Figure 7**: Partial dependency plots showing the effect of each predictor variable: temperature

882 2 m above the bed (Temp 2 m), depth-mean backscatter intensity linearly (Backscatter),

883   temperature 50 m above the bed (Temp 50 m), upward (+ve) and downward (-ve) current

884   flow (Vertical velocity), time relative to high tide in steps of 5-min (0.083h) with high tide zero,

885   negative values before (flood) and positive values after (ebb) (Time to high tide), near-surface

886   current 48.5 m above the bed (depth 17.6 m) flowing 117° (-ve) and 297° (+ve) relative to N

887   (Longshore (u) 48.5 m), near bed current 8.5 m above the bed (depth 57.6 m) flowing 117° (-

888   ve) and 297° (+ve) relative to N (Longshore (u) 8.5 m), near-surface current 48.5 m above the

889   bed (depth 17.6 m) flowing 27° (-ve) and 207° (+ve) relative to N (Cross-shore (v) 48.5 m),

890   near bed current 8.5 m above the bed (depth 57.6 m) flowing 27° (-ve) and 207° (+ve) relative

891   to N (Cross-shore (v) 8.5 m), on the occurrence of tagged *M. alfredi* at Manta Alley while

892   keeping all other variables at their mean. The green line shows smoothed partial decency.

893   Rugs display the distribution of the data for presence (top, blue), and absence (red, bottom).

894

895   **Data Accessibility**

896   The   data   that   supports   these   findings   are   available   from   FigShare   (doi:

897   10.6084/m9.figshare.13139309) following a one-year embargo from the date of publication

898   to allow for further publication of research findings.

899

900   **Competing Interests**

901   There are no competing financial, professional, or personal interests that might have

902   influenced the performance or presentation of the work described in this manuscript.

903   **Author contributions**

904 **Joanna L. Harris**: Conceptualisation; data curation; formal analysis; investigation;

905 methodology; project administration; software; visualisation; writing – original draft

906 preparation; writing – review & editing. **Phil Hosegood**: Conceptualisation; investigation;

907 project administration; supervision; writing – review & editing. **Edward Robinson**: Data

908 curation; software; investigation; writing – review & editing. **Clare B. Embling**: Supervision;

909 writing – review & editing. **Simon Hilbourne**: Investigation; writing – review & editing. **Guy**

910 **M. W. Stevens:** Conceptualisation; supervision; writing – review & editing.

911

Acknowledgements

921

Authors' Contributions

923 Joanna Harris: Conceptualization-Lead, Data curation (lead); Formal analysis (lead);

924 Investigation (lead); Methodology (lead); Writing-original draft (lead); Writing-review &

925 editing (lead). Phil Hosegood: Conceptualization (supporting); Funding acquisition (equal);

926 Investigation (supporting); Project administration (lead); Supervision (equal); Writing-review

927 & editing (supporting). Edward Robinson: Data curation (supporting); Investigation

928 (supporting); Software (supporting); Writing-review & editing (supporting). Clare Embling:

929 Supervision (equal); Writing-review & editing (supporting). Simon Hilbourne: Investigation

930 (supporting); Writing-review & editing (supporting). Guy Stevens: Conceptualization

931 (supporting); Funding acquisition (equal); Supervision (equal); Writing-original draft

932 (supporting); Writing-review & editing (supporting).

933

934 **Conflict of Interest.**

935 None declared.
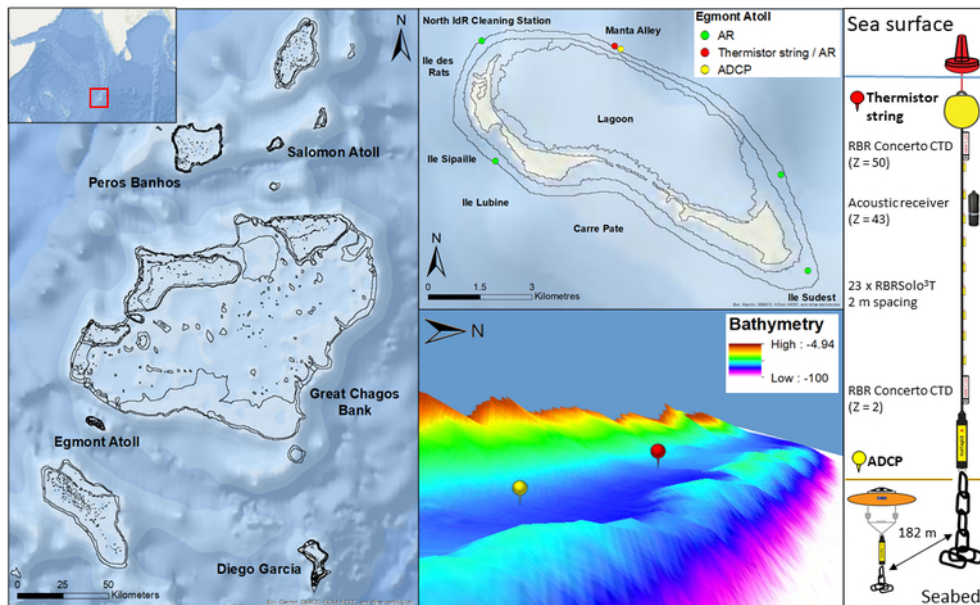
The Central Indian Ocean with Chagos Archipelago indicated within the red box (left inset). The Chagos Archipelago with Egmont Atoll indicated within the red box (left). Egmont Atoll and the location of the oceanographic and acoustic receiver mooring in Manta Alley (red and yellow dots) and four acoustic receivers (green dots) (top right). Bathymetric view of Manta Alley obtained via multibeam survey (Robinson and Hosegood *et al.*, unpublished data) showing the location of the moorings (bottom right). Bottom right legend showing instrument configurations of the long thermistor string (red dot/pin) and subsurface ADCP moorings (yellow dot/pin) deployed 182 m apart anchored at a depth of 66 m. Z is the height above the seabed.

33x22mm (600 x 600 DPI)

Reef manta rays (*Mobula alfredi*) engaged in feeding activities at the Manta Alley feeding aggregation site in north Egmont Atoll.

169x113mm (600 x 600 DPI)
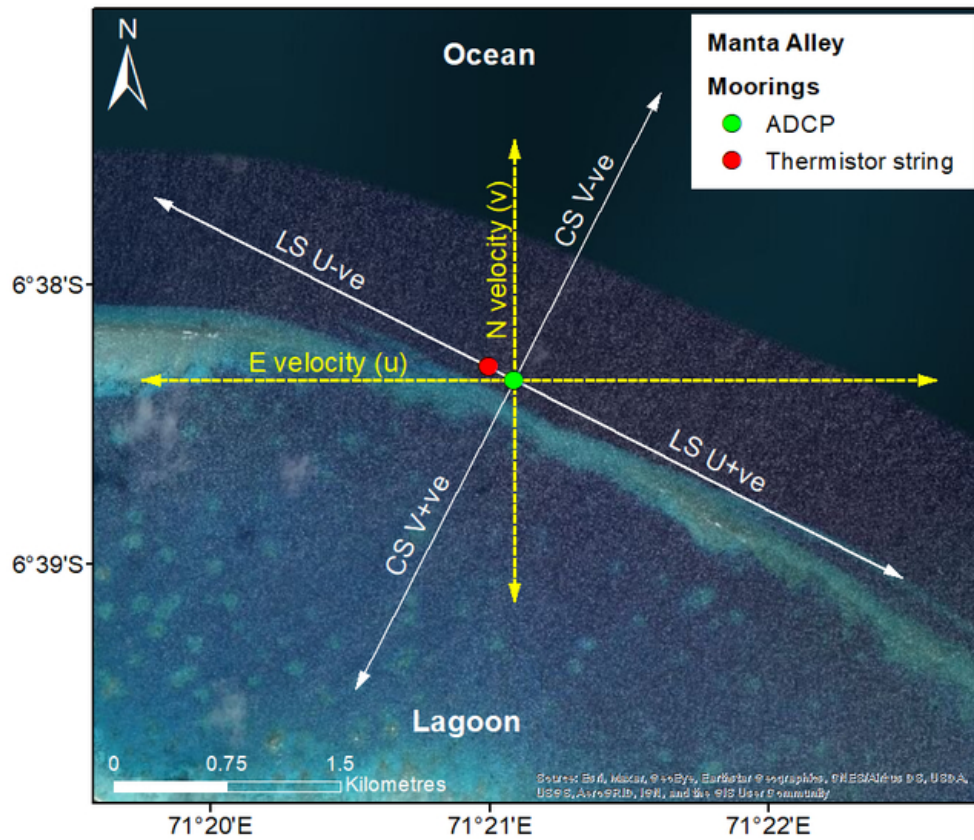
Original current u and v components (yellow dashed lines) and after clockwise rotation 117° relative to north (white lines). Arrows on the white lines show the direction of longshore u (LS U-ve and LS U+ve) and cross-shore v (CS V-ve and CS V+ve). Showing mooring locations: long thermistor string (red dot) and subsurface ADCP moorings (yellow dot).

27x25mm (600 x 600 DPI)
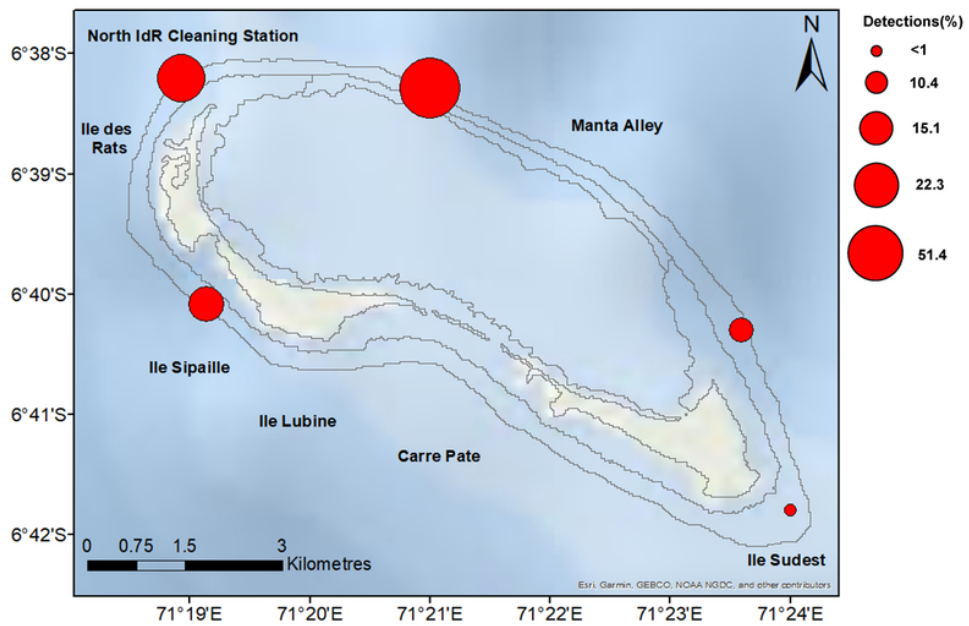
Percentage of detections at each site.

34x22mm (600 x 600 DPI)
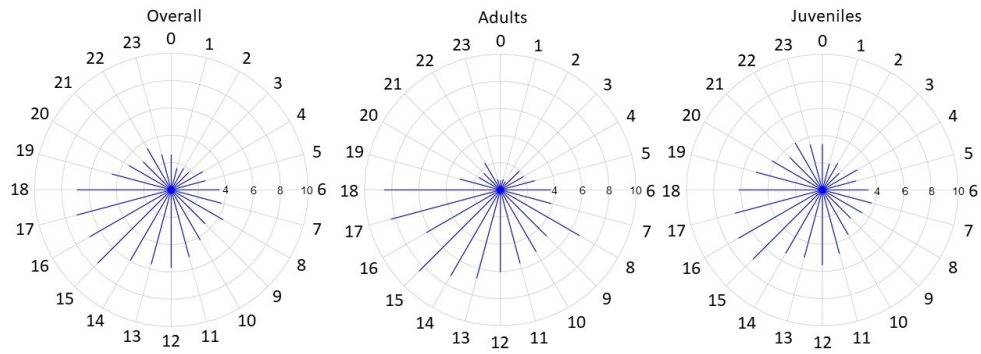
Percentage distribution of detections by hour of the day at Egmont Atoll for all tagged *M. alfredi* (left), adults only (middle) and juveniles only (right).
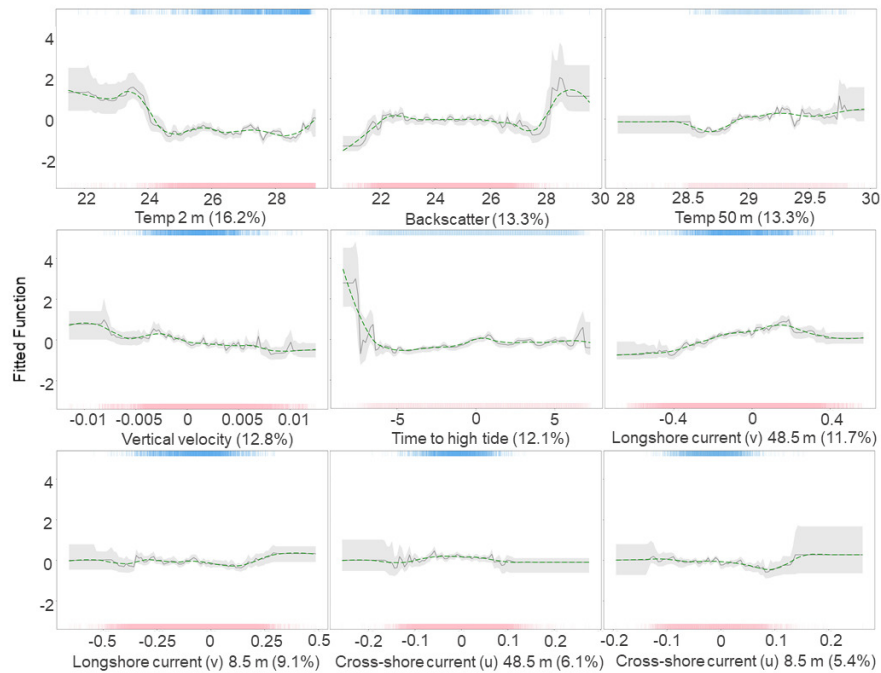
108x48mm (300 x 300 DPI)

Resident events at each site showing location (by colour) and time at the location (by size).

40x22mm (600 x 600 DPI)

Partial dependency plots showing the effect of each predictor variable: temperature 2 m above the bed (Temp 2 m), depth-mean backscatter intensity linearly (Backscatter), temperature 50 m above the bed (Temp 50 m), upward (+ve) and downward (-ve) current flow (Vertical velocity), time relative to high tide in steps of 5-min (0.083h) with high tide zero, negative values before (flood) and positive values after (ebb) (Time to high tide), near-surface current 48.5 m above the bed (depth 17.6 m) flowing 117° (-ve) and 297° (+ve) relative to N (Longshore (u) 48.5 m), near bed current 8.5 m above the bed (depth 57.6 m) flowing 117° (-ve) and 297° (+ve) relative to N (Longshore (u) 8.5 m), near-surface current 48.5 m above the bed (depth 17.6 m) flowing 27° (-ve) and 207° (+ve) relative to N (Cross-shore (v) 48.5 m), near bed current 8.5 m above the bed (depth 57.6 m) flowing 27° (-ve) and 207° (+ve) relative to N (Cross-shore (v) 8.5 m), on the occurrence of tagged *M. alfredi* at Manta Alley while keeping all other variables at their mean. The green line shows smoothed partial decency. Rugs display the distribution of the data for presence (top, blue), and absence (red, bottom).
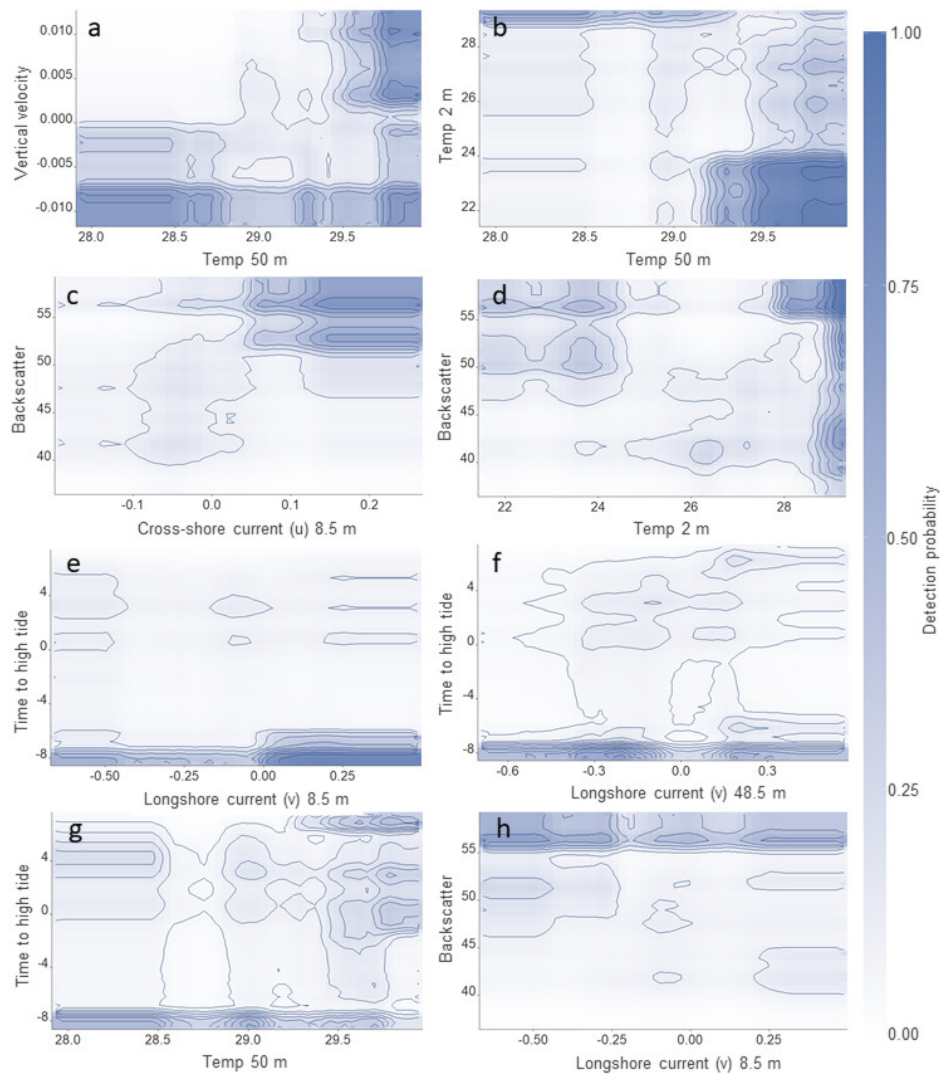
99x67mm (300 x 300 DPI)
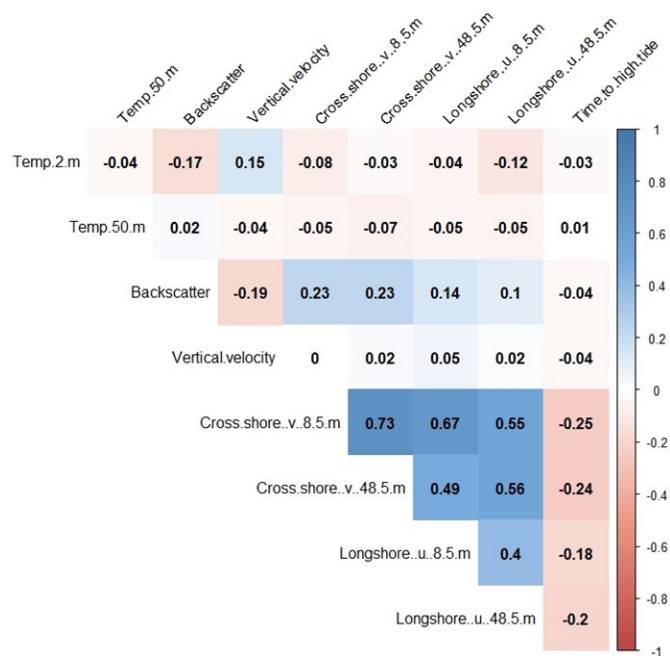
Correlation matrix for all predictors used in the boosted regression trees model.

88x60mm (300 x 300 DPI)

Pairwise interactions between predictor variables contour lines highlight the probability of *M. alfredi* tag detection at Manta Alley while keeping all other variables at their mean. All interactions were significant (*p<0.01*). Plot number related to the interaction effect shown in Table 3. A detailed description of each variable can be found in Table 1.

67x73mm (300 x 300 DPI)